Journal of Zhejiang University-SCIENCE A (Applied Physics & Engineering)
ISSN 1673-565X (Print); ISSN 1862-1775 (Online)
www.jzus.zju.edu.cn; www.springerlink.com
E-mail: jzus@zju.edu.cn

Numerical investigation of dynamic properties of plasma sheath with pitching motion

De-yang TIAN, Guo-chao FAN, Wei-fang CHEN[†‡]

School of Aeronautics and Astronautics, Zhejiang University, Hangzhou 310027, China

[†]E-mail: chenwfnudt@163.com

Received Sept. 28, 2019; Revision accepted Jan. 31, 2020; Crosschecked Feb. 25, 2020

Abstract: Research on the dynamic properties of a plasma sheath coupled with pitching motion of the vehicle has great significance in solving the problem of communication interruption in the process of vehicle reentry. This paper investigates the dynamic properties of the plasma sheath by using the simplified conventional Burnett (SCB) equations and the Navier-Stokes (NS) equations with the thermochemical non-equilibrium effect. The eleven-species chemical kinetic models are applied to the comparison and there is verification of a dynamic plasma sheath simulation for the first time. After the introduction of vehicle pitching motion, the dynamic results are more consistent with the experimental data than the simulated results when treating it as static state. The plasma sheath characteristic parameters show periodic properties, whose changing period is the same as the pitching motion period. However, because of different velocities of the pitching motion, phase shifts exist in different positions of the vehicle. The enhancement of the rarefied effect weakens the disturbance to the plasma sheath. This research reveals the distribution and regularities of the dynamic plasma sheath. It is significant in solving the ionization blackout problem and the design of the reentry vehicle, and provides reliable data for further research on the dynamic plasma sheath.

Key words: Plasma sheath; Dynamic; Thermodynamic non-equilibrium; Rarefied flow
https://doi.org/10.1631/jzus.A1900503 **CLC number:** V211

1 Introduction

The plasma sheath which is formed in front of the reentry vehicle is a special complex electromagnetic environment, which seriously restricts reliable information transmission (Yang et al., 2007). Comprehensive understanding of the dynamic properties of plasma sheath is the prerequisite to ensuring continuous navigation and communication coverage for a reentry vehicle. It has profound theoretical research significance and engineering application value (Akey and Cross, 1970). However, there are still some limitations in the understanding of the formation mechanism and distribution rules of the plasma sheath in a complex flow environment in adjacent space. The lack of relevant research methods has become a restriction on the development of information chain safety and target recognition technology of a vehicle in the environment of a dynamic plasma sheath (Li, 2005; Hu et al., 2006). In this context, exploring the plasma sheath environment of reentry vehicles and objectively understanding the distribution characteristics and variation rules are cutting-edge research projects and are urgent requirements for engineering application.

A lot of numerical investigations of plasma sheath for reentry vehicles, such as Radio Attenuation Measurement (RAM-C II) (Candler, 1988), the Apollo Command Module (Wright et al., 2004), and the Mars Space Laboratory (Edquist, 2005) have been studied and analyzed. Because of the lack of simulation methods, most studies consider the plasma

‡ Corresponding author
ORCID: De-yang TIAN, https://orcid.org/0000-0002-7325-738X

sheath covering the reentry vehicle to be static, but in the real reentry environment, the plasma sheath is definitely dynamic (Piziali, 1994).

With the development of computational fluid dynamics and computer technology, numerical simulation has gradually become the main means of studying the distribution and dynamic properties of the plasma sheath for a reentry vehicle (Ohler et al., 1999; Scalabrin and Boyd, 2006; Yang et al., 2013). Most research is based on the Navier-Stokes (NS) equation, but recently some have tried to apply the simplified conventional Burnett (SCB) equations to the simulation of thermochemical non-equilibrium rarefied flow (Zhong et al., 1993). The objective of this paper is to reveal the distribution and regularities of the dynamic plasma sheath. The numerical simulation methods of the plasma flow field are constructed based on SCB equations and NS equations. Numerical comparison and verification are carried out by different chemical reaction kinetics models (seven-/eleven-species Gupta/Dunn & Kang/Park finite rate chemical kinetics models) at altitudes of 71 km and 81 km, and adaptability analysis is carried out on each model and of its influence on the plasma flow field.

2 Governing equations

The governing equations of a plasma flow field based on NS equations can be summarized as

$$\frac{\partial \boldsymbol{Q}}{\partial t}+\frac{\partial \boldsymbol{E}}{\partial x}+\frac{\partial \boldsymbol{F}}{\partial y}+\frac{\partial \boldsymbol{G}}{\partial z}+\frac{\partial \boldsymbol{E}_{\mathrm{v}}}{\partial x}+\frac{\partial \boldsymbol{F}_{\mathrm{v}}}{\partial y}+\frac{\partial \boldsymbol{G}_{\mathrm{v}}}{\partial z}=\boldsymbol{S}, \quad (1)$$

where t is the time, $\boldsymbol{E}$, $\boldsymbol{F}$, $\boldsymbol{G}$, $\boldsymbol{E}_{\mathrm{v}}$, $\boldsymbol{F}_{\mathrm{v}}$, and $\boldsymbol{G}_{\mathrm{v}}$ are the inviscid and viscous components in the x, y, and z directions, $\boldsymbol{Q}$ is a conserved variable, and $\boldsymbol{S}$ is the chemical source. The specific expansion forms are as follows:

$$\begin{aligned}
\boldsymbol{Q}&=\left[\rho C_i, \rho u, \rho v, \rho w, \rho E, \rho e_{\mathrm{vib}}\right]^{\mathrm{T}},\\
\boldsymbol{E}&=\left[\rho C_i u, \rho u^2+p, \rho uv, \rho uw, (\rho E+p)u, \rho e_{\mathrm{vib}}u\right]^{\mathrm{T}},\\
\boldsymbol{F}&=\left[\rho C_i v, \rho uv, \rho v^2+p, \rho vw, (\rho E+p)v, \rho e_{\mathrm{vib}}v\right]^{\mathrm{T}},\\
\boldsymbol{G}&=\left[\rho C_i w, \rho uw, \rho vw, \rho w^2+p, (\rho E+p)w, \rho e_{\mathrm{vib}}w\right]^{\mathrm{T}},\\
\boldsymbol{E}_{\mathrm{v}}&=\left[-\rho D_i\frac{\partial C_i}{\partial x}, \tau_{xx}, \tau_{yx}, \tau_{zx}, q_x+q_{\mathrm{vib}x}\right.\\
&\quad \left.+u_i\tau_{xi}-\rho\sum_{i=1}^{n_{\mathrm{s}}}D_i h_i\frac{\partial C_i}{\partial x}, q_{\mathrm{vib}x}-\rho\sum_{i=1}^{\mathrm{mol}}D_i e_{\mathrm{vib}}^i\frac{\partial C_i}{\partial x}\right]^{\mathrm{T}},\\
\boldsymbol{F}_{\mathrm{v}}&=\left[-\rho D_i\frac{\partial C_i}{\partial y}, \tau_{xy}, \tau_{yy}, \tau_{zy}, q_y+q_{\mathrm{vib}y}\right.\\
&\quad \left.+u_j\tau_{yj}-\rho\sum_{i=1}^{n_{\mathrm{s}}}D_i h_i\frac{\partial C_i}{\partial y}, q_{\mathrm{vib}y}-\rho\sum_{i=1}^{\mathrm{mol}}D_i e_{\mathrm{vib}}^i\frac{\partial C_i}{\partial y}\right]^{\mathrm{T}},\\
\boldsymbol{G}_{\mathrm{v}}&=\left[-\rho D_i\frac{\partial C_i}{\partial z}, \tau_{xz}, \tau_{yz}, \tau_{zz}, q_z+q_{\mathrm{vib}z}\right.\\
&\quad \left.+u_k\tau_{zk}-\rho\sum_{i=1}^{n_{\mathrm{s}}}D_i h_i\frac{\partial C_i}{\partial z}, q_{\mathrm{vib}z}-\rho\sum_{i=1}^{\mathrm{mol}}D_i e_{\mathrm{vib}}^i\frac{\partial C_i}{\partial z}\right]^{\mathrm{T}},\\
\boldsymbol{S}&=\left[\dot{\omega}_i, 0, 0, 0, 0, \dot{\omega}_{\mathrm{vib}}\right]^{\mathrm{T}},
\end{aligned} \quad (2)$$

where ρ is the density of the gas mixture, E is the electric field intensity, e_{vib} is the vibrational energy per unit mass, p is the pressure, C_i is the species mass fraction, D_i is the diffusion coefficient, $\boldsymbol{\tau}$ is the stress tensor, u, v, and w are the velocities in the x, y and z directions, q_x, q_y, and q_z are the translational-rotational heat in the x, y, and z directions, $q_{\mathrm{vib}x}$, $q_{\mathrm{vib}y}$, and $q_{\mathrm{vib}z}$ are the vibrational heat flux terms in the x, y, and z directions, respectively, n_{s} is the number of components, mol is molecule, h_i is the enthalpy, $\dot{\omega}_i$ is species production rate, and $\dot{\omega}_{\mathrm{vib}}$ is the source term of vibrational energy and electronic energy.

To simulate rarefied flow, the conventional Burnett (CB) equations are introduced here. These have a higher order constitutive relation than the NS equations by the Chapman-Enskog expansion (Chapman, 1916; Wang and Uhlenbeck, 1948). Taking into account calculation efficiency, some second-order stress terms of the CB equations can be neglected in hypersonic flow because of the dimensional analysis. Therefore, the SCB equations (Zhao et al., 2015) are used, and these are applicable to the simulation of hypersonic rarefied flow. The high-order stress and heat flow terms can be written as

$$\begin{aligned}
\tau_{ij}=\tau_{ij}^{(1)}+\tau_{ij}^{(2)}&=-2\mu\overline{\frac{\partial u_i}{\partial x_j}}+K_1\frac{\mu^2}{p}\frac{\partial u_k}{\partial x_k}\overline{\frac{\partial u_i}{\partial x_j}}\\
&\quad +K_2\frac{\mu^2}{p}\left(-\overline{\frac{\partial u_k}{\partial x_i}\frac{\partial u_j}{\partial x_k}}-2\overline{\overline{\frac{\partial u_i}{\partial x_k}\frac{\partial u_k}{\partial x_j}}}\right)+K_6\frac{\mu^2}{p}\overline{\overline{\frac{\partial u_i}{\partial x_k}\frac{\partial u_k}{\partial x_j}}},
\end{aligned}$$

$$
\begin{aligned}
q_i = q_i^{(1)} + q_i^{(2)} = &-\kappa \frac{\partial T}{\partial x_i} + \theta_1 \frac{\mu^2}{\rho T} \frac{\partial u_k}{\partial x_k} \frac{\partial T}{\partial x_i} \\
&+ \theta_2 \frac{\mu^2}{\rho T} \left[\frac{2}{3} \frac{\partial}{\partial x_i} \left(T \frac{\partial u_k}{\partial x_k} \right) + 2 \frac{\partial u_k}{\partial x_i} \frac{\partial T}{\partial x_k} \right] \\
&+ \left(\theta_3 \frac{\mu^2}{\rho p} \frac{\partial p}{\partial x_k} + \theta_4 \frac{\mu^2}{\rho} \frac{\partial}{\partial x_k} + \theta_5 \frac{\mu^2}{\rho T} \frac{\partial T}{\partial x_k} \right) \overline{\frac{\partial u_k}{\partial x_i}},
\end{aligned} \tag{3}
$$

where μ is the viscosity coefficient, K_1, K_2, K_6, and θ_1–θ_5 are coefficients in the constitutive relation of Burnett's equations, T is the translational-rotational temperature, and κ is the ratio of the coefficient of heat conduction to the coefficient of viscosity.

3 Chemical kinetic models

A chemical kinetic model is the key point of numerical simulation for a plasma flow field. For hypersonic flow, the commonly used air reaction models mainly include five-, seven-, and eleven-species models. The five-species reaction model is mainly used in the flow field of a chemical reaction without ionization of gas, and the species involved are O, N, NO, N_2, and O_2. Since we are focusing on the plasma sheath, the five-species model is not applicable. The seven-species model is mostly used in the high-speed flow field with a velocity of about 7 km/s, and the species involved are O, N, NO, N_2, O_2, NO^+, and e. According to the calculation states, the seven-species model is the most appropriate. The eleven-species model is mostly used for reentry flight flow fields with a velocity of about 11 km/s, and the species involved are O, N, NO, N_2, O_2, O_2^+, N_2^+, O^+, N^+, NO^+, and e.

$k_{\mathrm{f},j}$ is the forward reaction rate and $k_{\mathrm{b},j}$ is the backward reaction rate, defined by the Arrhenius equation. The calculation expressions are:

$$
\begin{aligned}
k_{\mathrm{f},j} &= A_{\mathrm{f},j} T^{B_{\mathrm{f},j}} \exp\left(-\frac{E_{\mathrm{f},j}}{T} \right), \\
k_{\mathrm{b},j} &= A_{\mathrm{b},j} T^{B_{\mathrm{b},j}} \exp\left(-\frac{E_{\mathrm{b},j}}{T} \right),
\end{aligned} \tag{4}
$$

where the values of A_f, B_f, E_f and A_b, B_b, E_b are determined by Gupta's air reaction model.

For a multicomponent chemical reaction, the chemical reaction formula and the corresponding forward and backward reaction rates must be determined to obtain the formation rate of the components. Dunn and Kang (1973), Park (1985), and Gupta et al. (1990) all proposed their own reaction and temperature models. The Gupta model provides the eleven-species chemical reaction rate table of air, and contains 20 reaction formulas in total, and the data of the first seven reaction formulas are used for the seven-species. The Dunn & Kang model contains 26 reaction formulas, and the data of the first 12 reaction formulas are used for the seven-species. The Park model contains 21 reaction formulas, and the data of the first 11 reaction formulas are used for the seven-species.

4 Numerical computation methods

The finite volume method (Mazumder, 2016) is used for the numerical computations. The advection upstream splitting method by pressure-based weight function (AUSMPW+) (Kim et al., 2001) is used for spatial discretization. The implicit lower-upper symmetric Gauss-Seidel relaxation (LU-SGS) (Yoon and Jameson, 1986, 1987) with double time steps is used for time discretization.

Since the calculated states belong to the rarefied flow, the first-order Maxwell slip velocity boundary condition is used for the surface boundary condition. The free flow boundary condition is used for the supersonic inflow boundary condition, and extrapolation interpolation processing is used for the outflow boundary condition. The simulation results of the steady flow field are taken as the initial value of the dynamic flow field.

5 Calculation conditions

The experiments on the RAM-C II vehicle focus on the plasma sheath distributions, and are widely used in the comparison and verification of hypersonic vehicle flow field simulation algorithms. The blunt cone RAM-C II model's ball head radius is R_n= 0.1524 m, half cone angle is 9°, and the total length is 1.295 m. The computational grid of the vehicle is

shown in Fig. 1. The inlet velocity in the test is 7650 m/s (Walters et al., 1992; Boyd, 2007; Andrienko et al., 2014). To quantify the distribution of the plasma sheath, points *A* and *B* are selected on the vehicle. Point *A* locates at x/R_n=1, and point *B* locates at x/R_n=7. The calculation conditions are given in Table 1.

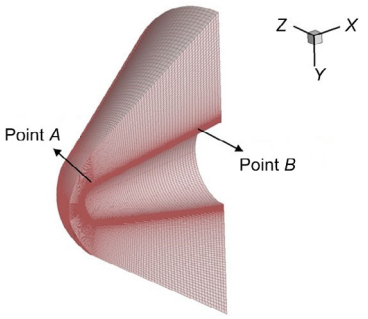

Fig. 1 Computational grid of RAM-C II vehicle

Table 1 Calculation conditions

Parameter	Value	
	Case a	Case b
Altitude (km)	71	81
Velocity (m/s)	7650	7650
Mach No.	25.9	28.3
Angle of attack (°)	±2	±2
Frequency (Hz)	100	100
Density (kg/m^3)	7.19×10^{-5}	1.57×10^{-5}
Temperature (K)	216.846	196.686

The sinusoidal pitching motion is defined as

$$\alpha = \alpha_{\max} \sin(2\pi f t), \tag{5}$$

where α is the time-varying angle of attack, $\alpha_{\max}$ is the pitching motion amplitude, and f is the pitching motion frequency. The time step is $\Delta t=10^{-6}$ s.

It is generally considered that the result of numerical simulation converges when the residuals decrease by 4 to 5 orders of magnitude. Fig. 2 shows the residual convergence curve of dynamic simulation results at the altitude of 71 km. This example was calculated for more than 40 000 steps, and the convergence curve of the electron mass fraction is also given. The convergence curves show that the calculated results have converged very well, and would ensure the accuracy of results.

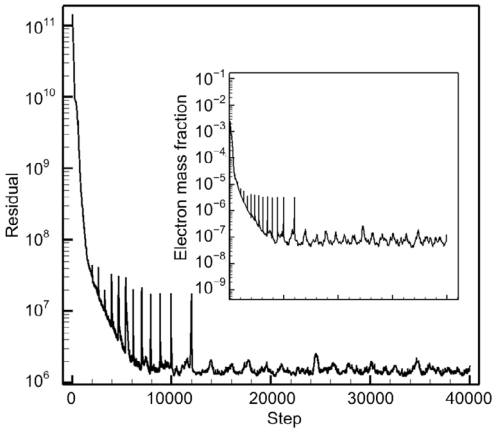

Fig. 2 Convergence curves of residual and electron mass fraction

The grid independence for the numerical simulation of the pitching motion vehicle is analyzed by three different grids. The coarse grid sizes (axial× normal) are 60×80 nodes. The medium grid sizes are 80×100 nodes, and the fine grid sizes are 100×120 nodes. Fig. 3 shows the distribution of heat flow (Q_{dot}) under three different grid conditions at the altitude of 71 km. The results show that the coarse grids cannot predict the heat flow correctly. The results show little difference between medium and fine girds. To improve the computational efficiency, the medium grids with 80×100 nodes are selected for the dynamic pitching motion simulation.

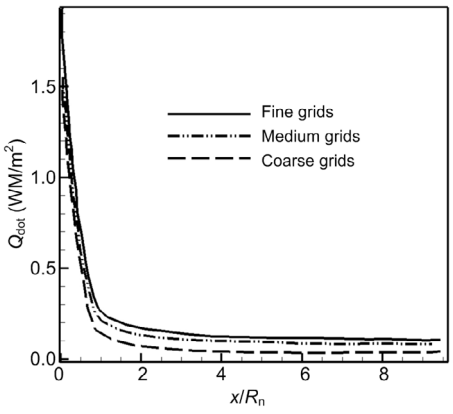

Fig. 3 Heat flow distribution of RAM-C II vehicle

6 Simulation results and discussion

To study the formation mechanism of the plasma sheath, the numerical simulation of a steady plasma

sheath is carried out. Figs. 4 and 5 intuitively show that as the flight height increases, SCB equations acquire thicker shock waves than NS equations, and therefore the characterization of the plasma sheath is more accurate. The results calculated by the SCB equations are superior to those of the NS equations in the rarefied flow region. As can be seen from Fig. 5, there is a significant difference between translational-rotational temperature (T) and vibrational temperature (T_v) behind the shock wave region. It indicates that there is an obvious translation-vibration non-equilibrium phenomenon in this region. The translation-vibration non-equilibrium effect is significantly enhanced with the increase of flight altitude, which indicates that the rarefaction degree of the inflow increases with the increase of altitude. The effects of rarefied gas on the chemical reaction non-equilibrium and thermodynamic non-equilibrium are different.

Numerical comparison and verification are carried out by different chemical reaction kinetics models (seven-/eleven-species Gupta/Dunn & Kang/ Park finite rate chemical models) at altitudes of 71 km and 81 km, and the adaptability analysis is performed on each model and of its influence on the plasma flow field. As shown in Figs. 6 and 7, from the contours of the temperature distribution, the results calculated by different chemical models and different species air reaction models are different. The thickness of the shock wave calculated by the seven-species air reaction models is greater than that calculated by the eleven-species air reaction models. In order to more carefully compare the advantages and disadvantages of several models, the peak value of electron density along the axis of RAM-C II vehicle is given below, so that it can be analyzed with quantitative data and experimental data.

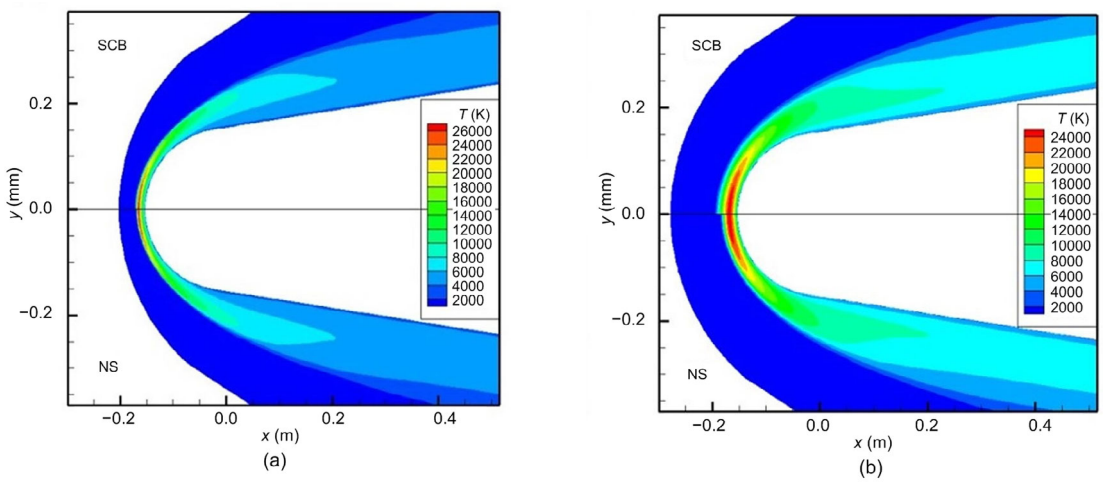

Fig. 4 Contours of temperature for RAM-C II vehicle at 71 km (a) and 81 km (b)

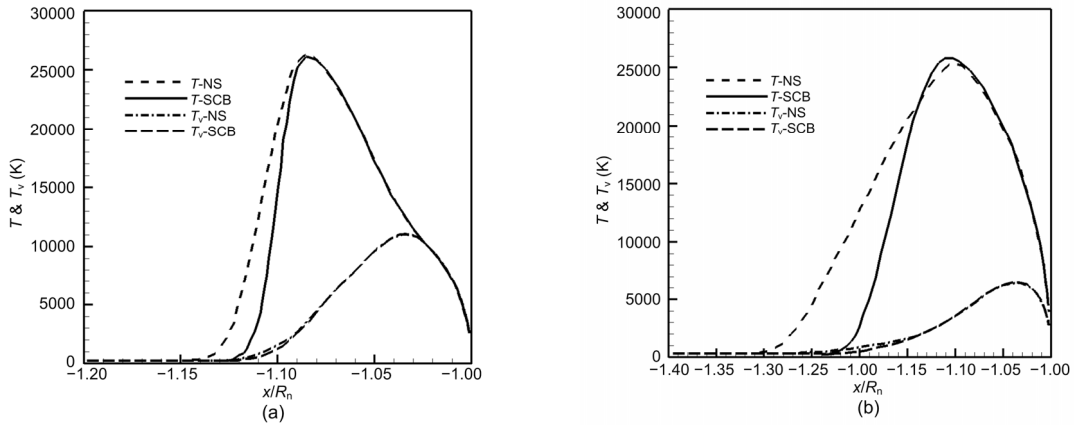

Fig. 5 Translational-rotational and vibrational temperature distributions along the stagnation at 71 km (a) and 81 km (b)

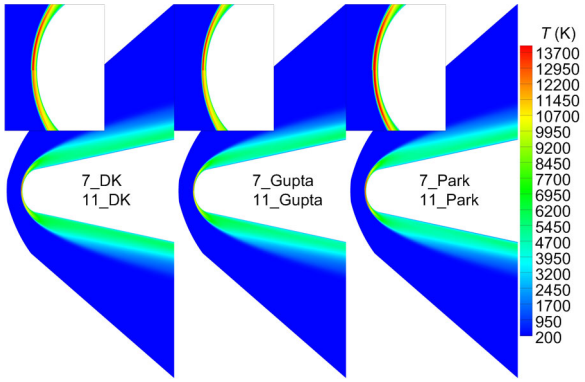

Fig. 6 Contours of temperature for RAM-C II vehicle at 71 km

7: seven-species; 11: eleven-species; DK: Dunn & Kang model; Gupta: Gupta model; Park: Park model

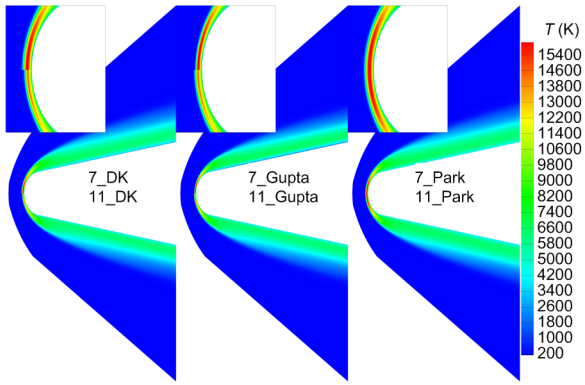

Fig. 7 Contours of temperature for RAM-C II vehicle at 81 km

As shown in Fig. 8, at the altitude of 71 km, for the seven-species model, the error between the peak value of electron number density at each section calculated by the Dunn & Kang and Gupta models and the experimental data is within half an order of magnitude, while the error of the Park model is within one order of magnitude. At the altitude of 81 km, for the seven-species model, the error between the peak value of electron number density at each section calculated by the Dunn & Kang model and the experimental data is within half an order of magnitude, while the error of the Gupta and Park models is within an order of magnitude. For the eleven-species model, the results calculated by the Dunn & Kang, Gupta, and Park models are significantly different at the altitudes of 71 km and 81 km, but the eleven-species results of the Park model are more similar to the seven-species results of other models. From the above results, the seven-species Gupta model and Park two-temperature model are adopted for subsequent numerical simulation of the dynamic plasma sheath with pitching motion in order to improve computational efficiency.

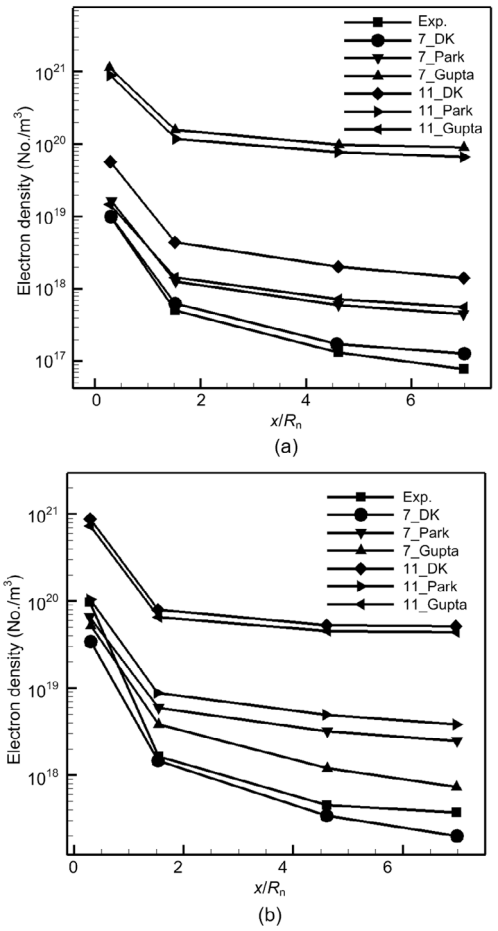

Fig. 8 Peak value of electron number density in each chemical reaction model at 71 km (a) and 81 km (b)

Under the condition of rarefied flow, the aircraft pitching motion can still induce significant dynamic characteristics of the plasma sheath. The time-varying curves of plasma characteristic parameters at points *A* and *B* at altitudes of 71 km and 81 km after 13 pitching motion periods and corresponding attack angles of the aircraft are given in Fig. 9. The rarefied gas effect resulted in a significant increase in the difference of plasma collision frequency between the shoulder region and the body region of the reentry vehicle. The collision frequency exhibits the same periodic time-varying regularity as the pitching

motion frequency of the vehicle at the altitude of 71 km and 81 km. However, because of different velocities of pitching motion, the phase shifts existed in different positions of the vehicle. In addition, the higher pitching motion velocity of the vehicle still does not cause additional disturbance to the characteristic frequency of the wall plasma.

Fig. 10 shows the plasma collision frequency normal to the surface at the altitude of 71 km and 81 km. T' is the period of pitching motion. It can be clearly seen that the dynamic results are more consistent with the experimental data than the simulated results when treating it as a steady state, and more accurate plasma collision frequencies are obtained. With the increase of flight altitude, the thickness of plasma boundary layer at 71 km and 81 km increased, and the change gradient of the collision frequency along the normal direction of the object surface is significantly reduced. The difference of steady state space plasma collision frequency at different angles of attack gradually decreases with the increase of flight altitude. The maximum relative deviations of steady state of 2° and −2° angles of attack and steady state of 0° angle of attack at 81 km are 21.8% and 23.6%, respectively.

7 Conclusions

Comprehensive understanding of the dynamic properties of the plasma sheath is a prerequisite for hypersonic reentry vehicle navigation and communication. In this study, the method of steady and dynamic plasma sheath simulation for rarefied flow is proposed. The results calculated by SCB equations with thermochemical non-equilibrium effect are

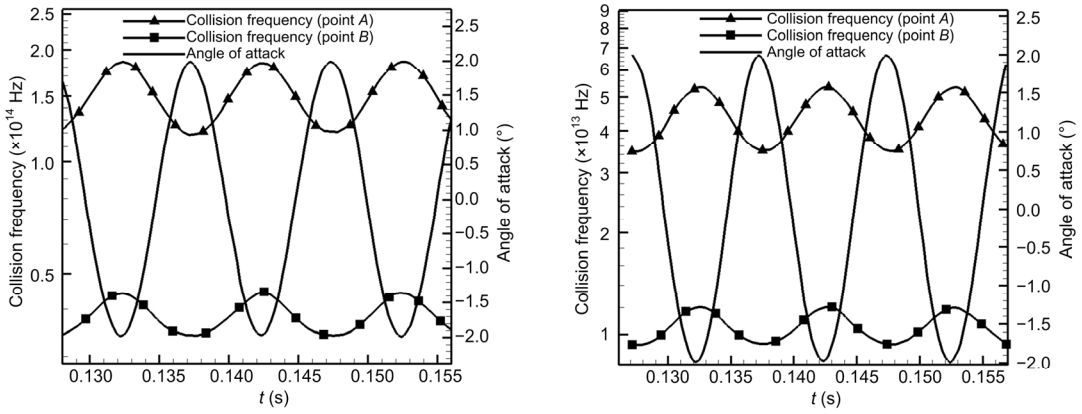

Fig. 9 Plasma collision frequency for RAM-C II vehicle at 71 km (a) and 81 km (b)

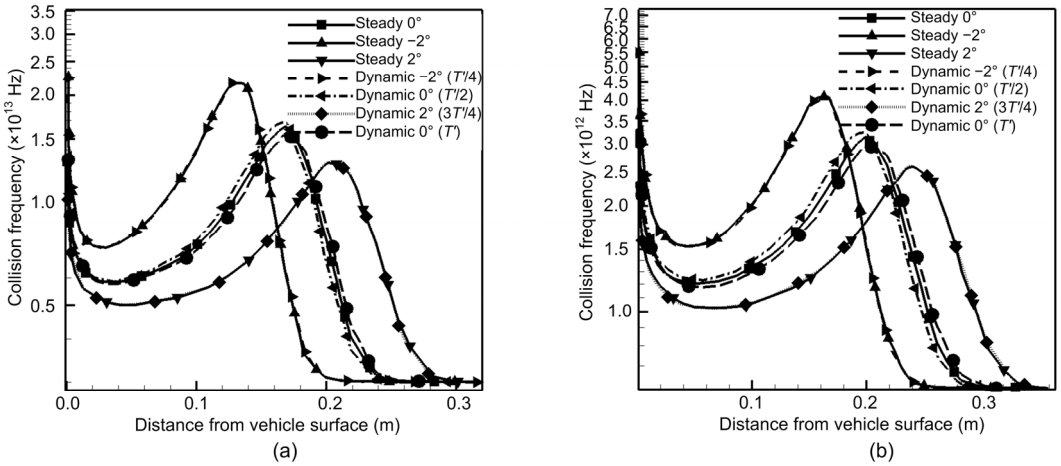

Fig. 10 Plasma collision frequency normal to the surface at 71 km (a) and 81 km (b)

superior to those from NS equations in the rarefied flow condition. The shock waves predicted by the SCB equations are thicker, which leads to the initial position of the chemical reaction of air species farther away from the surface, and also have an obvious influence on the description of the characteristic parameters of the plasma sheath.

The numerical comparison and verification are carried out by different chemical reaction kinetics models. The results calculated by the seven-species Gupta model are superior to the other models, and the errors are within half an order of magnitude.

Finally, the dynamic results are more consistent with the experimental data than the simulated results when treating it as in steady state. The plasma sheath characteristic parameters show periodic properties, where the changing period is the same as the pitching motion period, but it has a phase delay in the body region because of the higher pitching motion velocity. With the increase of flight altitude, the rarefaction effect leads to an increase of the molecular mean free path, and the chemical reaction gradually weakens and tends to freeze, which leads to the significant decrease of plasma concentration. The enhancement of the rarefied effect weakens the disturbance to the plasma sheath caused by the vehicle pitching motion.

This research reveals the distribution and regularities of the dynamic plasma sheath. It has significance for solving the ionization blackout problem and the design of the reentry vehicle, and provides more reliable data for further research on the dynamic plasma sheath. However, this paper only studies the dynamic characteristics of the plasma sheath with pitching motion. More forms of dynamic properties can be studied to gain a more comprehensive understanding.

Contributors

De-yang TIAN designed the research. De-yang TIAN and Guo-chao FAN processed the corresponding data. De-yang TIAN wrote the first draft of the manuscript. Guo-chao FAN and Wei-fang CHEN helped to organize the manuscript. De-yang TIAN and Wei-fang CHEN revised and edited the final version.

Conflict of interest

De-yang TIAN, Guo-chao FAN, and Wei-fang CHEN declare that they have no conflict of interest.

References

Akey ND, Cross AE, 1970. Radio Blackout Alleviation and Plasma Diagnostic Results from a 25000 Foot per Second Blunt-body Reentry. NASA Technical Note, NASA TND-5615, National Aeronautics and Space Administration, Washington, USA.

Andrienko DA, Shang JS, Surzhikov ST, et al., 2014. Non-equilibrium flow field of RAM-C II probe. Proceedings of the 45th AIAA Plasmadynamics and Lasers Conference. https://doi.org/10.2514/6.2014-2376

Boyd ID, 2007. Modeling of associative ionization reactions in hypersonic rarefied flows. *Physics of Fluids*, 19(9):096102. https://doi.org/10.1063/1.2771662

Candler GV, 1988. The Computation of Weakly Ionized Hypersonic Flows in Thermo-chemical Nonequilibrium. PhD Thesis, Stanford University, California, USA.

Chapman S, 1916. On the law of distribution of molecular velocities, and on the theory of viscosity and thermal conduction, in a non-uniform simple monatomic gas. *Philosophical Transactions of the Royal Society A: Mathematical, Physical and Engineering Sciences*, 216(538-548):279-348. https://doi.org/10.1098/rsta.1916.0006

Dunn MG, Kang S, 1973. Theoretical and Experimental Studies of Reentry Plasmas. NASA CR-2232, National Aeronautics and Space Administration, Washington, USA.

Edquist KT, 2005. Afterbody heating predictions for a Mars science laboratory entry vehicle. Proceedings of the 38th AIAA Thermophysics Conference. https://doi.org/10.2514/6.2005-4817

Gupta RN, Yos JM, Thompson RA, et al., 1990. A Review of Reaction Rates and Thermodynamic and Transport Properties for an 11-Species Air Model for Chemical and Thermal Nonequilibrium Calculations to 30000 K. NASA STI/Recon Technical Report N, NASA, Washington, USA.

Hu HJ, Liu J, Ma M, 2006. Radar and USB capture and track the re-entry module in the black block area. *Manned Spaceflight*, (3):49-53 (in Chinese).

Kim KH, Kim C, Rho OH, 2001. Methods for the accurate computations of hypersonic flows: I. AUSMPW+scheme. *Journal of Computational Physics*, 174(1):38-80. https://doi.org/10.1006/jcph.2001.6873

Li DH, 2005. Development of main mission antenna system of Shenzhou spacecraft. *Journal of Manned Space*, (3):23-27 (in Chinese).

Mazumder S, 2016. Numerical Methods for Partial Differential Equations. Academic Press, New York, USA, p.277-338. https://doi.org/10.1016/B978-0-12-849894-1.00006-8

Ohler SG, Gilchrist BE, Gallimore AD, 1999. Electromagnetic signal modification in a localized high-speed plasma flow: simulations and experimental validation of a stationary plasma thruster. *IEEE Transactions on Plasma Science*, 27(2):587-594. https://doi.org/10.1109/27.772290

Park C, 1985. Problems of rate chemistry in the flight regimes of aeroassisted orbital transfer vehicles. *In*: Nelson HF (Ed.), Progress in Astronautics and Aeronautics: Thermal Design of Aeroassisted Orbital Transfer Vehicles. AIAA, New York, USA, p.511-537.

Piziali RA, 1994. 2-D and 3-D Oscillating Wing Aerodynamics for a Range of Angles of Attack Including Stall. NASA TM 4632, National Aeronautics and Space Administration, Washington, USA.

Scalabrin LC, Boyd ID, 2006. Numerical simulation of weakly ionized hypersonic flow for reentry configurations. Proceedings of the 9th AIAA/ASME Joint Thermophysics and Heat Transfer Conference. https://doi.org/10.2514/6.2006-3773

Walters RW, Cinnella P, Slack DC, et al., 1992. Characteristic-based algorithms for flows in thermochemical nonequilibrium. *AIAA Journal*, 30(5):1304-1313. https://doi.org/10.2514/3.11065

Wang CS, Uhlenbeck GE, 1948. On the transport phenomena in rarefied gases. *Studies in Statistical Mechanics*, 5:1-17.

Wright MJ, Prabhu DK, Martinez ER, 2004. Analysis of afterbody heating rates on the Apollo command modules, part I: AS-202. Proceedings of the 37th AIAA Thermophysics Conference. https://doi.org/10.2514/6.2004-2456

Yang HW, Tang WC, Kong XK, 2007. Calculation of the effect on the reflection of the plane electromagnetic wave for non-magnetized plasma with different electron density distributions. *International Journal of Infrared and Millimeter Waves*, 28(7):547-556. https://doi.org/10.1007/s10762-007-9226-8

Yang LX, Shen DH, Shi WD, 2013. Analyses of electromagnetic scattering characteristics for 3D time-varying plasma medium. *Acta Physica Sinica*, 62(10):104101 (in Chinese). https://doi.org/10.7498/aps.62.104101

Yoon S, Jameson A, 1986. A Multigrid LU-SSOR Scheme for Approximate Newton Iteration Applied to the Euler Equations. NASA Contractor Report 179524, National Aeronautics and Space Administration, Washington, USA.

Yoon S, Jameson A, 1987. An LU-SSOR scheme for the Euler and Navier-Stokes equations. Proceedings of the 25th AIAA Aerospace Sciences Meeting. https://doi.org/10.2514/6.1987-600

Zhao WW, Chen WF, Agarwal RK, 2015. Computation of rarefied hypersonic flows using modified form of conventional Burnett equations. *Journal of Spacecraft and Rockets*, 52(3):789-803. https://doi.org/10.2514/1.A33059

Zhong XL, MacCormack RW, Chapman DR, 1993. Stabilization of the Burnett equations and application to hypersonicflows. *AIAA Journal*, 31(6):1036-1043. https://doi.org/10.2514/3.11726

中文概要

题　目： 俯仰运动下等离子鞘套动态特性数值研究

目　的： 通过对俯仰运动情况下的钝锥体等离子鞘套进行数值模拟，揭示动态等离子鞘套的分布规律，提高数据的可靠性，为进一步研究入射电磁波与动态等离子鞘套的相互作用机理提供有力依据，并为再入飞行器黑障问题的解决和再入飞行器设计提供参考。

创新点： 考虑热化学非平衡效应的简化常规 Burnett（SCB）方程能够更准确地描述再入飞行器等离子鞘套的动态分布规律。

方　法： 1. 提出稀薄流域稳态与动态等离子鞘套数值模拟方法；2. 对不同化学反应动力学模型和热力学模型进行数值比较和验证；3. 引入俯仰运动后对再入飞行器等离子鞘套的动态特性进行数值模拟。

结　论： 1. 在稀薄流条件下 SCB 方程模拟得到的激波更厚，对等离子鞘套的刻画更为准确精细。2. 7 组元 Gupta 化学反应模型与 Park 双温模型的计算结果优于其他模型。3. 引入俯仰运动后，飞行器不同位置的碰撞频率等关键参数与俯仰运动的周期存在相位差；同时增强稀薄效应将减弱俯仰运动对动态等离子鞘套的扰动。

关键词： 等离子鞘套；动态；热力学非平衡；稀薄流